Energy & Buildings 167 (2018) 240–252

Contents lists available at ScienceDirect

Energy & Buildings

journal homepage: www.elsevier.com/locate/enbuild

A numerical study of adaptive building enclosure systems using solid–solid phase change materials with variable transparency

Gert Guldentops[a,d], Giuseppe Ardito[a], Mingjiang Tao[a], Sergio Granados-Focil[b], Steven Van Dessel[c,*]

[a] Department of Civil and Environmental Engineering, Worcester Polytechnic Institute, 100 Institute Rd, MA, Worcester, 01609, USA
[b] Department of Chemistry, Clark University, 950 Main St, MA, Worcester, 01610, USA
[c] Architectural Engineering Program, Department of Civil and Environmental Engineering, Worcester Polytechnic Institute, 100 Institute Rd, MA, Worcester, 01610, USA
[d] Simpson Gumpertz & Heger Inc., 41 Seyon St Building 1 Suite 500, MA, Waltham, 02453, USA

ARTICLE INFO

Article history:
Received 17 September 2017
Revised 8 January 2018
Accepted 22 February 2018
Available online 19 March 2018

Keywords:
Passive thermal control
Solid–solid phase change material
Finite element analysis
Transparency shift

ABSTRACT

Buildings currently consume about 40% of all energy use in the US and therefore play an important role in mitigating global greenhouse gas emissions. Passive solar design strategies can be used to limit building heating and cooling demands. Current passive solar design strategies, however, require substantial design effort for each individual project, often require mechanical and electrical control systems, and the approach is also difficult to implement in building retrofit projects. Solid–solid phase change materials (SS-PCM) are currently emerging as alternative materials for thermal energy storage. Here we present an exploratory study on two innovative climate responsive building enclosure systems that employ the transparency change and latent heat storage capacity of SS-PCMs as mechanisms to passively control building temperature. The first system is based on a thin layer of SS-PCM that is placed on top of a highly reflective film to control solar heat gain. The second system uses a layer of SS-PCM foam to store thermal energy and control heat flow. The performance characteristics of the systems are evaluated using finite element modeling techniques. Simulation results shed light on the synergistic interactions between different components of the systems and indicate that both systems can reduce undesirable heat exchange between the building and its environment if designed properly. Recommendations are made regarding various material and system parameters, including the attenuation coefficient of the SS-PCM, system thickness, void ratio and distribution of the void ratio of the SS-PCM foam based system, and phase transition temperature.

1. Introduction

World energy consumption is growing at an ever faster pace, thus driving the need for more efficient and sustainable energy technologies. Energy consumption in buildings currently stands at about 39% of total energy consumption in the United States, a significant portion of which is related to building heating and cooling loads [1,2]. The energy expended for thermal conditioning of buildings is largely affected by various heat transfer processes occurring across building enclosures. Common approaches to increase building envelope efficiency include the use of thermal insulation materials and radiative barriers, increasing overall envelope airtightness, use of shading devices to prevent excess solar heating, cross-ventilating buildings for thermal comfort, or incorporating latent heat storage materials to increase the ability to buffer diurnal thermal swings.

Passive Solar Façades are a family of building enclosure systems that use solar radiation to improve building thermal comfort and reduce energy use [3]. The term “passive” typically refers to those systems that rely on material-enabled control mechanisms, as opposed to “active” systems that rely on mechanical and/or electrical control devices [4]. An overview of climate responsive building enclosure systems, including both active and passive technologies, can be found in a recent review article [5]. Some notable examples include Trombe walls [6,7], transparent insulation [8–11], and double skin façades [12,13]. While passive solar façades can reduce building energy use, they can be difficult to control [14–17] and are therefore often combined with active support systems to operate more effectively as hybrid systems [18–21], which increases their complexity. Implementation of more elaborate passive solar

* Corresponding author.
E-mail address: svandessel@wpi.edu (S. Van Dessel).

https://doi.org/10.1016/j.enbuild.2018.02.054
0378-7788/

Nomenclature

Greek letters

α	surface absorptivity
κ	absorption coefficient
λ	wavelength
ρ	density or surface reflection
Σ	building enclosure tilt angle
θ	angle
ε	surface emissivity
φ	surface azimuth

Index

β-CD	β-cyclodextrin
A	amorphous
a	air
app	apparent
B	specular solar component
C	crystalline
c_p	specific heat capacity
D	diffuse solar component
d	direction
dp	dewpoint
ext	external
f	forced convection
G	diffuse reflected solar component
G	irradiance
H	enthalpy
h	on a horizontal plane
h	surface heat transfer coefficient
I	forward radiative intensity
i	solar incidence
int	interior
J	backward radiative intensity
k	thermal conductivity
N	opaque sky cover
n	natural convection
n	refractive index
pc	of the phase transition
RH	relative humidity
s	scattering coefficient
T	temperature
t	time
v	velocity
w	wind
z	solar zenith
cell-g-PEG	cellulose and poly(ethylene glycol)
Hc	crystallization enthalpy
Hm	melting enthalpy
htr	heating rate
MDI	methylene diphenyl diisocyanate
NPG	neopentyl glycol
PEG	poly(ethylene glycol)
PEG	poly(ethylene glycol)
PSMA	poly(styrene-co-maleic anhydride)
PUPCM	polyurethane phase change material
SAN-g-PA	poly(styrene-co- acrylonitrile) and Palmitic acid
TAM	trihydroxy methyl-aminomethane
Tc	crystallization peak temperature
Tm	melting peak temperature

façades (such as double-skin facades) is also challenging in existing buildings, which are responsible for the bulk of building energy use. The design of passive solar façades also tends to be highly context-specific and thus demands advanced designer-skills, which increases cost [22–24]. These factors tend to hinder the widespread use of passive solar façades in buildings today, thus intensifying the need for developing new and innovative building envelope solutions.

Some passive solar façade systems employ thermal energy storage (TES) systems to compensate the effect of diurnal changes in outdoor temperature and solar energy. Sensible heat storage in common building materials or water has been a popular choice as they offer low cost solutions [25]. Phase change materials (PCM) have gained in popularity as they provide higher heat storage density and also allow for a better control over the amount of heat being released [25–28]. These so called latent heat storage materials absorb and release heat when undergoing a phase change, for example, from solid to liquid or vice versa. Solid–liquid PCMs (SL-PCM) are commonly used for TES in buildings, which include paraffins, salt hydrates, and various mixtures. SL-PCMs have also been used in passive solar facade systems where they can help with a more efficient bridging of periods with low solar irradiation. Some of the challenges of using SL-PCMs however include a need for containment when in liquid state (to avoid leakage), phase segregation (in mixtures), hysteresis, and low thermal conductivity [29,30].

Solid–solid PCMs (SS-PCM) are currently emerging as alternative TESs as they avoid some of the problems associated with their solid–liquid counter-parts [31]. SS-PCMs retain their bulk solid properties within certain temperature ranges, thus avoiding the need for encapsulation. SS-PCMs also experience less phase separation, degradation, and hysteresis upon thermal cycling [32–35]. In addition to these benefits, SS-PCMs have structural properties and can thus be more readily integrated as functional components of façade systems. For example, SS-PCMs can be applied closer to the building envelope surface where most of the heat exchange occurs. This may increase their capacity for thermal buffering without a need for high thermal conductivity. An overview of different types of SS-PCMs, including their respective properties, is presented in a recent review article [31]. Table 1 provides typical thermal properties values for some common SS-PCMs.

A promising example of an SS-PCM, which have been recently developed by the authors, entails the grafting of phase changing pendant motifs onto a polymeric backbone, as shown in Fig. 1. In such an SS-PCM, the pendants have the ability to undergo crystalline-amorphous phase changes which allows them to absorb and release latent heat upon thermal cycling. The SS-PCM material uses a polymethacrylate backbone containing alkyl pendant phase changing motifs (PSMA, see Table 1). The polymer is opaque when crystalline and becomes transparent when heated above its phase transition temperature (i.e. amorphous phase). The material exhibits a phase transition at 36 °C with a 10 °C wide hysteresis, and a latent heat capacity of 46 kJ/kg. Further alterations on these highly tunable polymer structures, by adding a flexible spacer between the polymer backbone and the crystallizing motif, result in significant increases in their latent heat capacities. An overview of different types of SS-PCMs, including their respective property ranges, is presented in a recent review article [31].

Here we investigate the potential use of SS-PCM in two innovative passive solar façade systems which may be used in existing or new buildings, and have the ability to adapt themselves in a passive manner to changes in the exterior environment. The goal of this approach is to attain improvements in building indoor comfort levels while also reducing building energy use. The proposed systems aim to take advantage of the unique properties of the SS-PCM, such as its shape stability and ability to change transparency with changes in temperature. We anticipate that a synergistic interaction between the SS-PCM and other components of the system, such as thin-film reflectors or absorbers, will lead to building enclosure systems that can passively adapt to external stimuli. The

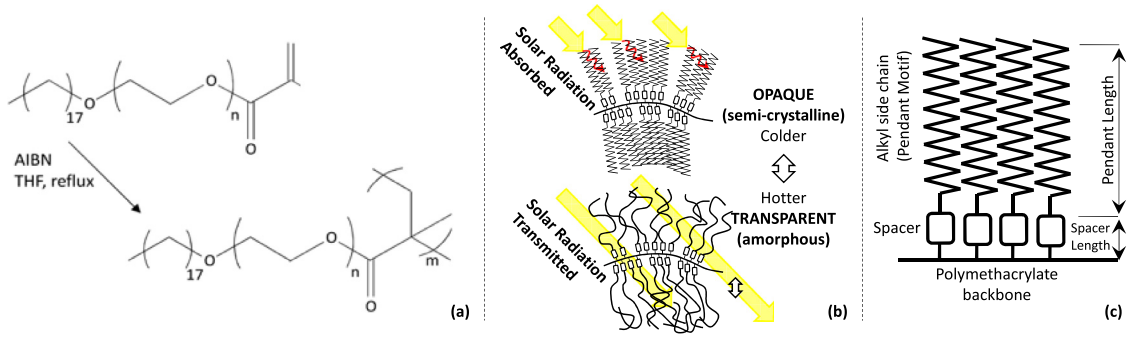

Fig. 1. Schematic representation of the molecular structure of the SS-PCM. a) Synthesis of polymeric SS-PCM, b) The alkyl side chains, with conformational freedom with ability to transition between a semi-crystalline (opaque) and amorphous (transparent) structure, c) schematic representation of polymer backbone with phase changing pendant side chains and spacers.

overall objective of this study is to understand the synergistic interactions among the components of the proposed facade systems for maximizing energy savings in buildings.

A detailed description and conceptual principles of the proposed systems are presented in Section 2. A parametric study was performed using a finite element model to investigate the potential energy reductions that could be achieved, and to provide insight into the sensitivity of the different system parameters. The methodology and numerical model is discussed in Section 3. Results of our study are presented in Section 4. Discussion and conclusions are provided in Sections 5 and 6 respectively.

2. Conceptual systems

Two building enclosure systems are proposed, which are described in detail in the next two sections: one is based on a thin layer of SS-PCM while the other is based on a thicker layer of SS-PCM foam. The components of each of the systems are first introduced, followed by the explanation of their respective working principles and hypothetical mechanisms of operations, and the synergistic interactions among the components. Both systems can respond passively to external stimuli (i.e., temperature) by the inclusion of an SS-PCM, which changes from transparent to opaque when it changes phases. This feature allows the systems to control the admittance of solar energy based on outside temperature, which enables their functioning as a thermochromic (TC) device. The use of SS-PCMs as a TC device differentiates this approach from previous thermochromic or electrochromic materials used in building enclosures [36–39].

The performance of the two technologies was compared to reference wall systems consisting of similar lightweight structures with equivalent thermal resistance. Both building enclosure systems were designed to reduce energy consumption in buildings by minimizing the overall undesirable heat exchange for a given time period. Undesirable heat exchange across the wall (expressed in kWh/m^2 for a reference time period) is used as the performance criteria, with a value of zero representing a perfect wall with zero-energy demand. All cases include a 75 mm insulation backing layer with the same thermal resistance. For the thin SS-PCM layer system with reflector, the reference case includes an opaque plastic layer at the outer surface. For the SS-PCM foam system, the reference case includes a 50 mm opaque foam in front of the insulation backing layer with the same thermal conductivity and thickness as the SS-PCM foam. The reference walls are almost identical in composition to the systems being investigated, however they include no TES or TC capabilities and the difference in performance is thus solely attributed to these added performance features.

2.1. Thin SS-PCM Layer + Reflector

The first system is based on a thin layer of SS-PCM that is placed to the exterior of a building envelope, which consists of the following functional layers (see Fig. 2): 1. an exterior surface; 2. a 1 mm thin SS-PCM layer; and 3. a back reflector made from a highly reflective thin film, such as aluminum or Mylar. In addition, an opaque 75 mm insulation backing is assumed behind the SS-PCM system for the numerical simulations (detailed in Section 3).

The hypothetical operational principles of the system to reduce undesirable heat exchange are explained as follows: 1. During winter, the SS-PCM is crystalline at low temperatures and remains opaque to solar radiation; and thus the exterior surface reflectance (or surface absorptance) of solar irradiance can be tuned to allow for more solar heat gains in winter; and 2. the SS-PCM becomes amorphous and transparent after it changes phase when heated above its phase transition temperature during summer. Consequently, the back reflector becomes exposed to solar irradiance and reflects all the solar irradiance that has not been reflected by the exterior surface. Our initial anticipation is that such a system benefits building energy performance for both summer and winter seasons.

2.2. SS-PCM foam system

The second building enclosure system explored in this study is based on a SS-PCM foam, which is comprised of the following functional layers (illustrated schematically in Fig. 3): 1. a structured front layer to passively control reflection or transmission of solar light during summer and winter, solstices respectively; and 2. a 50 mm foamed (cellular) SS-PCM with variable translucency. In addition, an opaque 75 mm insulation backing is assumed behind the SS-PCM foam system.

The working principles of the SS-PCM foam based system are postulated as follows: 1. The low thermal conductivity of SS-PCM, especially in cellular form, would significantly reduce or delay the heat loss from the interior space to the exterior during winter, and thus this feature prolongs the systems ability to keep a building at desired temperature; 2. The SS-PCM foam will absorb and store some solar radiation, which offsets some of the winter heat losses; 3. Latent heat capacity of the SS-PCM foam is employed to buffer heat gains to prevent overheating and the generation of excess summer heat gains; and 4. The synergistic interactions between 1, 2 and 3, and also the temperature dependent translucency and attenuation effect of the SS-PCM foam, will help reduce undesirable heat exchanges between interior and exterior spaces.

Passive control features may also be embedded into the structured front layer, in order to control the admittance of solar energy as a function of the solar incidence angle, which varies with season.

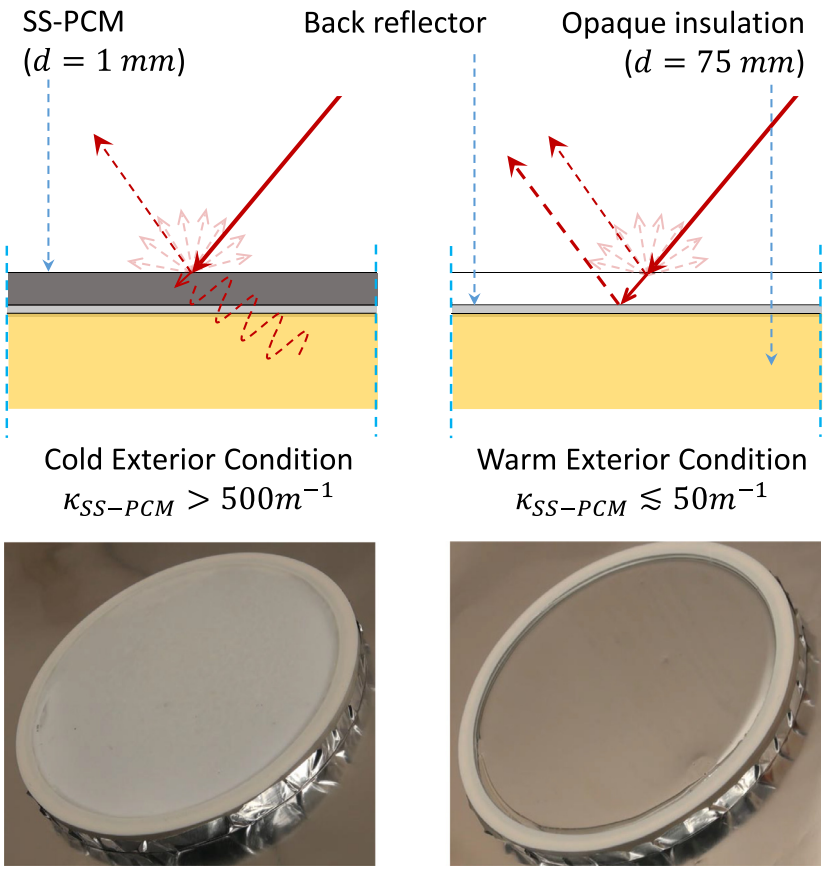

Fig. 2. Top: Conceptual working principles of a thin-layered system with variable reflectance, based on a SS-PCM with variable transparency. Left: SS-PCM thin-film is cold, crystalline, and opaque, causing considerable absorption of solar irradiance. Right: SS-PCM thin layer transitions to a transparent, amorphous, state, allowing for considerable reflection through the action of the reflector behind the SS-PCM. Bottom: SS-PCM opacity change from opaque (left) to transparent (right) with exposure of the reflective film.

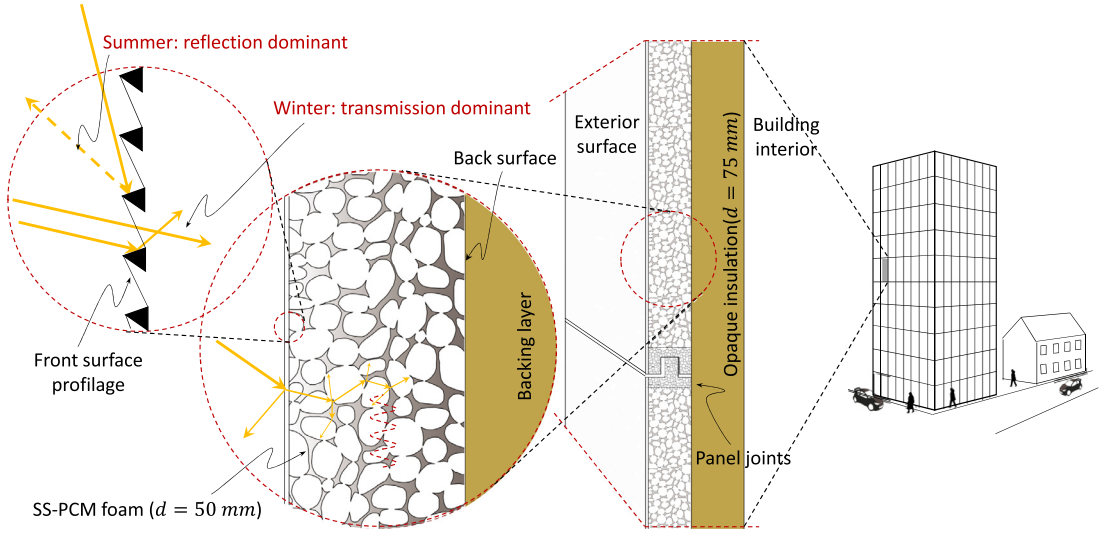

Fig. 3. Conceptual schematic of the SS-PCM foam system.

Both SS-PCM systems have to satisfy challenging requirements for minimizing undesirable heat exchanges during both winter (i.e., heat loss) and summer seasons (i.e., heat gains). The performance of both systems depends on the synergistic interaction between different system properties, which is not straight forward and thus FEM simulations (detailed in Section 3) were performed to identify what combinations of system parameters could deliver specific levels of energy savings.

3. Methodology

An exploratory study was performed to assess the feasibility of the proposed SS-PCM based facade systems in terms of energy savings. Using computational modeling, as a first step, the study focuses on the influence of system parameters on the heat transfer processes during the coldest and warmest weeks of the year.

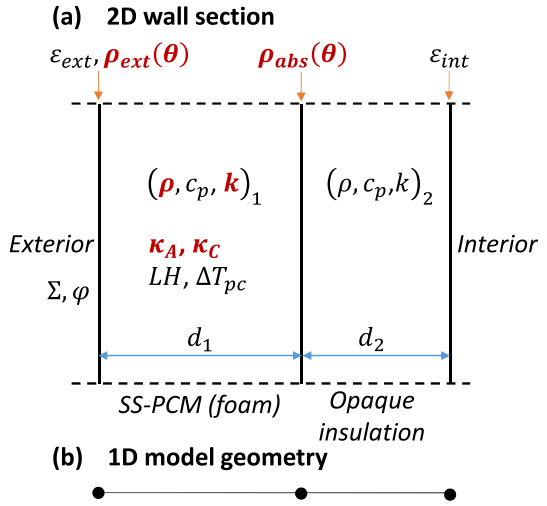

Fig. 4. (a): Schematic of the material properties and system parameters, (b): a schematic of the 1D geometry, required to compute the model. The parameters studied within this paper, see Paragraph 4, are depicted in bold and red. (For interpretation of the references to colour in this figure legend, the reader is referred to the web version of this article.)

3.1. Finite element modeling

FEM models were developed to simulate the heat transfer processes of the proposed building enclosure systems. The main objectives of the FEM modeling are: (i) to verify the feasibility of the two systems, (ii) to quantify the influence of material properties on thermal performance, and (iii) to provide insight and guidance to optimize the systems.

All problems discussed in this system can be simplified to a 1D geometry model, speeding up computations greatly. Fig. 4 gives an overview of both system input parameters, with exception of weather parameters, and a schematic of the 1D geometry.

3.1.1. Governing equations

The main governing equation employed by the numerical model is the heat equation (Eq. (1)) [40,41], as follows:

$$\rho c_p \frac{\partial T}{\partial t} = \nabla(k\nabla T) + \nabla \cdot q_r \tag{1}$$

The SS-PCM does not exhibit a significant flow regime, as all phases that are expected to be present, remain solid. Required here are the following material properties: density, ρ, specific heat capacity, c_p, and thermal conductivity, k.

However, the domain that represents the SS-PCM, will be transparent to solar radiation and is assumed to absorb some radiation within the medium, hence the addition of q_r in Eq. (1). In order to take this into account, a radiation in participating media Eq. (2) through (Eq. (5)) is added to the model [42]. These equations are derived from the Kubelka–Munk (KM) theory that considers the material as a slab absorbing (absorption coefficient, κ) and diffusing (scattering coefficient, s) solar radiation. The radiation field inside the translucent or transparent material layer consists of fluxes propagating in opposite directions. In the two flux model, the intensities of the diffuse fluxes traveling in the forward $I(x)$ and backward $J(x)$ directions at depth x along the spatial axis [43]. In the more rigorous four-flux KM model implemented here, radiation within the medium consists out of two specular and two diffuse fluxes propagating in opposite directions [44]. According to Vargas and Niklasson [45], the four-flux model compares well with numerical solutions of the equation of radiative transfer or with highly accurate Monte Carlo simulations [46,47].

$$\frac{dI_B}{dx} = -(\kappa + s)I_B + sJ_B \tag{2}$$

$$\frac{dJ_B}{dx} = -sI_B + (\kappa + s)J_B \tag{3}$$

$$\frac{dI_D}{dx} = -2[\kappa + s(1-f)]I_D + 2s(1-f)J_D + sfI_B \tag{4}$$

$$\frac{dJ_D}{dx} = 2[\kappa + s(1-f)]J_D - 2s(1-f)I_D + s(1-f)I_B \tag{5}$$

The KM theory was applied with different parameters in each layer, and can provide the total reflectance and absorptance of the solar irradiance. κ and s are both defined as a function of temperature and can be different in every cell of the translucent or transparent material layer. This allows us to capture the effect of the exact temperature gradient within the building enclosure on the level of translucency exhibited by the material. The coefficients κ and s in Eq. (2) through Eq. (5) should, therefore, be replaced with $\kappa(x, T)$ and $s(x, T)$ respectively. This is left out for the sake of clarity. The effect of refraction of solar radiation, which increases the length of the path traveled by the radiation flux, is incorporated within the model by multiplying κ by a coefficient.

The SS-PCM domain contains a modified heat capacity value in order to incorporate the effect of phase transition. This apparent heat capacity ($c_{p,\,app}$), is defined as follows:

$$c_{p,app} = C_{CorA}\frac{d}{dT}(H_{CtoA}) + (1 - C_{CorA})\frac{d}{dT}(H_{AtoC}) \tag{6}$$

Here, H represents enthalpy, which is defined as a function of temperature. Each direction of phase transition exhibits a unique enthalpy curve, H, due to the effect of hysteresis (see Fig. 5). A binary variable, C_{CorA}, is defined for each element that keeps track of the current phase of the PCM. This allows the model to select the appropriate enthalpy curve and calculate the correct apparent heat capacity (Eq. (6)). Upon completion of a phase transition, the value of C_{CorA} is reversed. The phase transition is assumed to occur over a temperature range, ΔT_{pc}, as can be seen in Fig. 5.

The FE modeling framework utilizes two spectral bands (solar radiation 0.25 μm $< \lambda <$ 2.5 μm, and IR radiation, $\lambda \geq$ 2.5 μm). All optical properties are assumed independent of wavelength within each bandwidth. The solar radiation impinging on the exterior cover plate of the system is modeled as an external radiation source [48]. The power of the specular solar irradiance component, $G_B(\theta,\ t)$, on the external surface of the building enclosure is calculated as a function of the intensity on a horizontal plane, $G_B(h)$, the solar zenith angle, $\theta_z(t)$, and solar incidence angle, $\theta_i(t)$. These angles are calculated using equations reported by Meeus [49]. The power of the diffuse component, $G_D(t)$, on the external surface is calculated using an experimentally based model developed by Perez et al. [50,51], which factors in surface orientation and sky conditions. Radiation received by surfaces in the vicinity of the building enclosure is assumed to be partially and diffusely reflected, and subsequently received by the building enclosure surface [48].

3.1.2. Boundary conditions

Exterior surface BC: Surface reflections of solar radiation are calculated using Eqs. (7) and (8), for specular and diffuse solar radiation respectively. Angle dependency of solar irradiance and solar surface reflectivity is, therefore, maintained. All surface properties are assumed independent of incidence angle and wavelength.

$$I_B = \alpha(\theta_i)G_{B,0} \tag{7}$$

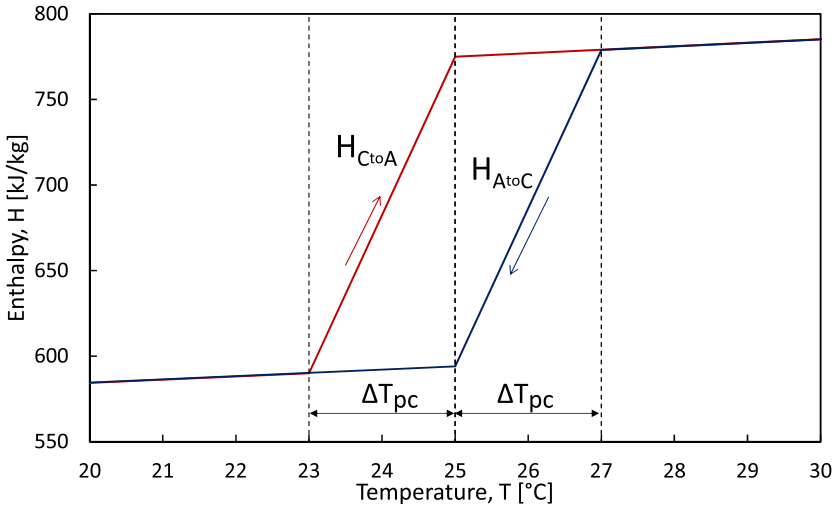

Fig. 5. Conceptual enthalpy curves regarding SS-PCM curves, which consider the effect of hysteresis during phase transition.

$$I_D = \int_{\theta=0}^{\Sigma-\frac{\pi}{2}} \alpha\left(\theta - \frac{\pi}{2} + \Sigma\right) G_{D,0}(\theta)\, d\theta + \int_{\theta=0}^{\Sigma} \alpha\left(\theta + \frac{\pi}{2} - \Sigma\right) G_{G,0}(\theta)\, d\theta \quad (8)$$

This takes care of the solar radiation bandwidth of the radiation mode of heat transfer. A supplementary boundary condition (Eq. (9)), is required for the IR radiation bandwidth. Since the external cover material can be assumed opaque to IR radiation, the Stefan–Boltzmann law is used to model this type of heat exchange. Kirchhoffs law ($\alpha_\lambda = \varepsilon_\lambda$) is also incorporated [42].

$$-\mathbf{n}\cdot(-k\nabla T) = \varepsilon\sigma\left[\left(\frac{1+\cos\Sigma}{2}\right)(T_{sky}^4 - T^4) + \left(\frac{1-\cos\Sigma}{2}\right)(T_{sur}^4 - T^4)\right] + h_{ext}(T_{a,ext} - T) \quad (9)$$

Models developed in [52] and [53] (Eqs. (10) and (11)) are used to estimate the sky radiative temperature, T_{sky}, which is used to calculate radiative heat exchange with the Earths atmosphere.

$$\varepsilon_{sky} = \left(0.787 + 0.764\ ln\left(\frac{T_{dp}}{273}\right)\right) \times (1 + 0.0224N - 0.0035N^2 + 2.8\cdot 10^{-4}N^3) \quad (10)$$

$$T_{sky} = \left(\frac{\varepsilon_{sky} T_{a,ext}^4}{\sigma}\right)^{\frac{1}{4}} - 273.15 \quad (11)$$

Here, the dewpoint temperature, T_{dp}, expressed in Kelvin, can be estimated accurately based on RH and $T_{a,\,ext}$ using a correlation found in [54]. The temperature of the externally surrounding surfaces, T_{sur}, is assumed equal to $T_{a,\,ext}$. Σ denotes the enclosure tilt angle.

The convection mode of heat transfer at the exterior surface of the building enclosure is modeled using Newtons law of cooling, see Eq. (9) [41]. The external convective heat transfer, h_{ext}, used in Eq. 9, exists out of two distinct parts, the first being forced convection, $h_{ext,\,f}$, and the second being natural convection, $h_{ext,\,n}$. $h_{ext,\,f}$ is derived using correlations that factor in surface-to-wind angle, w_d, and wind velocity, w_v, (Eq. (12)). These correlations have been derived using CFD tools [55] and have been validated using experimental data [56]. These do apply only for vertical or near vertical building enclosures.

$$\begin{aligned} h_{ext,f} &= 5.15(w_v)^{0.81} && 0^\circ \leqslant w_d < 22.5^\circ \\ h_{ext,f} &= 3.34(w_v)^{0.84} && 22.5^\circ \leqslant w_d < 67.5^\circ \\ h_{ext,f} &= 4.78(w_v)^{0.71} && 67.5^\circ \leqslant w_d < 112.5^\circ \\ h_{ext,f} &= 4.05(w_v)^{0.77} && 112.5^\circ \leqslant w_d < 157.5^\circ \\ h_{ext,f} &= 3.54(w_v)^{0.76} && 157.5^\circ \leqslant w_d < 180^\circ \end{aligned} \quad (12)$$

$h_{ext,\,n}$, on the other hand, is determined based on a correlation (Eq. (13)) derived as a function of the temperature difference and surface orientation [52].

$$h_{ext,n} = \frac{9.482|\Delta T|^{\frac{1}{3}}}{7.283 - |cos\,\Sigma|} \quad if\,\Delta T < 0\ upward, or\,\Delta T > 0\ downward$$

$$h_{ext,n} = \frac{1.810|\Delta T|^{\frac{1}{3}}}{1.382 + |cos\,\Sigma|} \quad if\,\Delta T > 0\ upward, or\,\Delta T < 0\ downward \quad (13)$$

Interior surface BC: The boundary at the interior side of the building enclosure is assigned in Eq. (14), which is similar to Eq. (9). Here, however, T_∞ is assumed equal to the internal air temperature, $T_{a,\,int}$, for both the convective and IR radiative exchange.

The internal convective heat transfer coefficient, h_{int}, is determined based on a correlation (Eq. (15)) derived using a large experimental test cell [57]. No forced convection is assumed here.

$$-\mathbf{n}\cdot(-k\nabla T) = \varepsilon\sigma\,(T_{a,int}^4 - T^4) + h_{int}(T_{a,int} - T) \quad (14)$$

$$h_{int} = \frac{2(T_{a,int} - T_{int})^{0.32}}{Height^{0.04}} \quad (15)$$

The necessary weather parameters to run the model are external air temperature, $T_{a,\,ext}$, relative humidity, RH, wind velocity, v_w, direction, d_w, and both specular, $G_{B,\,h}$, and diffuse, $G_{D,\,h}$, solar irradiance on a horizontal plane. The final necessary weather parameter is the opaque sky cover, N, clear sky ($N = 0$), complete overcast ($N = 1$), expressed in tenths. Geographic location and orientation of the system are also required.

3.1.3. Verification & validation

In order to verify the FE modeling framework, a grid study has been performed. In our case, grid independence is achieved when using linear elements with a constant length of 0.5 mm for the SS-PCM (foam). The same type of elements are used for the permanently opaque parts of the system as well, where their size ranges

Table 1
Thermal properties for different types of SS-PCMs [a] [31].

SS-PCM type			Tm [°C]	Hm [$\frac{J}{g}$]	Tc [°C]	Hc [$\frac{J}{g}$]	htr [$\frac{^{\circ}C}{min}$]
Polymeric		PSMA	36	46	26	45	2
	Grafted	SAN-g-PA	29–38	12–24	31–42	12–24	10
		cell-g-PEG	43–60	78–203	25–41	45–203	10
	Blocked	PUPCM β-CD	65	139	39	126	10
	Cross linked	MDI PEG	58–60	92–115	44–48	90–116	2
Organic	*Polyalcohol*	NPG TAM	36–39	27–143	22–30	33–150	5
		MDI PEG	60–61	121–132	45–46	116–121	–

a: See nomenclature for definition of terms used in Table 1.

Table 2
Assumed material and geometric properties for evaluation of both the thin SS-PCM layer system and SS-PCM foam system.

Layer/Material	*d*[mm]	$k\left[\frac{W}{m.K}\right]$	$c_p\left[\frac{kJ}{kg.K}\right]$	$\rho\left[\frac{kg}{m^3}\right]$	ρ^c_{ext}	ε	κ
Thin SS-PCM layer	1	0.16	2.3	930	*a*	0.9	*a*
Back reflector[d]	–	–	–	–	0.95	–	–
Insulation backing	75	0.03	1.5	21	–	0.9	–
SS-PCM foam	50	*b*	*b*	*b*	0.4	0.9	*a*
Blowing agent	–	0.014	–	–	–	–	–
SS-PCM	–	0.16	2.3	930	–	–	–
Absorber wall[d]	–	–	–	–	0.05	–	–
Insulation backing	75	0.03	1.5	21	–	0.9	–

a: studied parameter; *b*: function of the void ratio, which itself is a studied parameter; *c*: value in table represents reflection for irradiance with normal incidence angle; *d*: only optical properties are taken into account.

from 0.5 mm to 1.3 mm. A maximum time step of 15 min results in accurate interpolations of the solution in between time steps.

To validate the solution of the model, a comparison has been made between different modules of the FE model, such as the phase transition module, or the transparency module, and general known analytical solutions.

3.2. Parametric study: baseline & parameters

The proposed systems were evaluated for the on average coldest and warmest week of a typical meteorological year, for a central Massachusetts climate. This climate exhibits both an average high in July of 26.1 °C and an average low in January of −0.6 °C respectively. The building enclosure is south facing ($\varphi = 0^{\circ}$) vertical wall ($\Sigma = 90^{\circ}$), unless stated otherwise. The SS-PCM material exhibits a phase transition between 24 °C and 26 °C, thus exhibiting a 2 °C wide hysteresis, and a latent heat capacity of 180 kJ/kg.

A summary of the assumed system properties is provided in Table 2. Note that the chosen latent heat capacity and phase change temperature are within the typical value range of SS-PCM thermal properties reported in the literature.(See Table 1)

The exterior reflection coefficient, ρ_{ext}, and the attenuation coefficient for both crystalline and amorphous phases, are variables within the parametric study of the thin SS-PCM layer system. For the SS-PCM foam system, the aforementioned properties, as well as the foam void ratio, are studied. An overview of the required input parameters, with the exception of the weather parameters, is depicted in Fig. 4.

3.2.1. Parametric study: studied parameters and their range

In the SS-PCM thin film application, the exterior reflection coefficient, ρ_{ext}, and the attenuation coefficient of the SS-PCM thin film when amorphous (transparent), κ_A, are studied in the form of a parametric study. These two parameters are of the most interest because ρ_{ext} influences the amount of solar irradiance reflected at all times, whilst κ_A determines how thin the layer of SS-PCM needs to be and how much attenuation of solar irradiance still occurs within the thin-film SS-PCM. Within this parametric study, ρ_{ext} ranges from 0.2 to 0.8 for normal incidence angles, and κ_A ranges from 50 to 300 m^{-1}.

The performance of the SS-PCM foam based building enclosure system is influenced by many parameters. Attenuation of solar radiation within the SS-PCM foam is important in both the amorphous and crystalline phases of the SS-PCM. The SS-PCM foams void ratio influences its thermal conductivity and heat storage capacity, as well as the attenuation of solar radiation within the SS-PCM foam. A low attenuation will allow more solar radiation to be absorbed deeper into the foam, while a high attenuation leads to more absorption closer to the exterior surface. The former may be ideal in cold conditions, whilst the latter may be more desirable in summer conditions. The system parameters of most interest include both the amorphous and crystalline attenuation coefficients, κ_A and κ_C, of the SS-PCM foam. The void foam ratio, δ is used within this work to represent the amount of blowing agent as a fraction of the total volume of foam. Equations reported by Glicksman [58] are used to calculate thermal conductivity as a function of the foam void ratio and material properties of both the blowing agent and the SS-PCM. Although ρ_{ext} is also important, as it influences the amount of solar irradiance absorbed by the foam at its outer surface, it was not included within the parametric study as we focused primarily on the influencing factors attributed to the SS-PCM foam itself. κ_A and κ_C range from 50 to 350 m^{-1} and 500 to 3000 m^{-1} respectively. δ ranges from 0.65 to 0.95, and we also evaluated a SS-PCM foam with a non-uniform foam void ratio (see Fig. 6). A nonuniform δ will result in a nonuniform attenuation within the foam. A higher δ will cause more attenuation in the form of scattering, rather than absorption, when the foam is translucent (amorphous). A lower δ will lead to a higher attenuation due to more absorption because of more solid material when the material is opaque (translucent). The thickness of the SS-PCM foam system is set at 50 mm, which was applied on top of a 75 mm traditional thermal insulation layer. The reference case is a 125 mm traditional thermal insulation system (50 mm plus 75 mm).

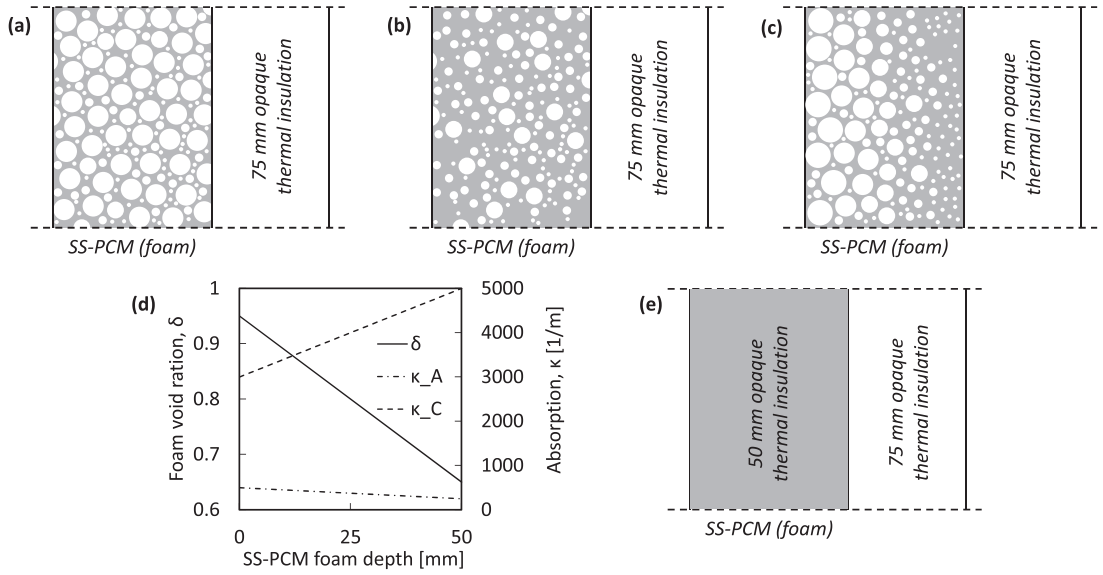

Fig. 6. Three types of SS-PCM foam systems were studied: (a) a uniform lightweight foam, (b) a uniform high density foam, and (c) a non-uniform foam with low density (high foam void ratio) at the exterior surface and high density (low foam void ratio) near the absorber wall. All SS-PCM foam systems are placed in front of 75 mm (conventional) opaque thermal insulation, (d) Distribution of foam void ratio and amorphous and crystalline attenuation at different SS-PCM foam depths, (e) Reference wall composed of 50 mm + 75 mm (conventional) opaque thermal insulation.

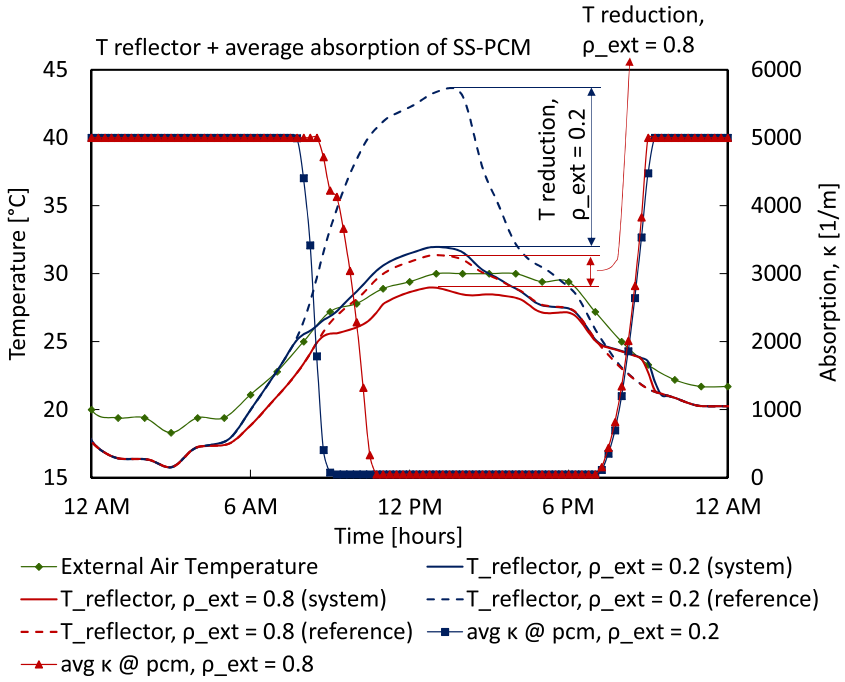

Fig. 7. Thin SS-PCM Layer + Reflector: Diurnal cycle of back reflector temperature and average attenuation coefficient, κ, of the SS-PCM, for both a low and a high external reflection coefficient, ρ_{ext}.

4. Results

4.1. Thin SS-PCM Layer + Reflector

The exterior reflection coefficient, ρ_{ext}, as well as the attenuation coefficient of the SS-PCM during its amorphous (transparent) phase, κ_A, have significant influence on the potential energy savings delivered by the system. Here we present results on the influence of these two material properties. The assumed material properties and system parameters are provided in Paragraph 3.2 and Table 2.

Fig. 7 shows the temperature and absorption coefficient of the back reflector and thin SS-PCM layer respectively during a typical 24 h diurnal cycle for the on average warmest week of the year (summer) in central Massachusetts. During nighttime, the SS-PCM remains crystalline and the attenuation coefficient, κ_C, is, therefore, assumed to be 5000 m^{-1}. In the morning, when the external temperature rises, the SS-PCM becomes amorphous and its attenuation coefficient gradually decreases to a value of 50 m^{-1}. The reverse happens in the evening when external temperature falls below the SS-PCMs phase transition temperature (24/26 °C).

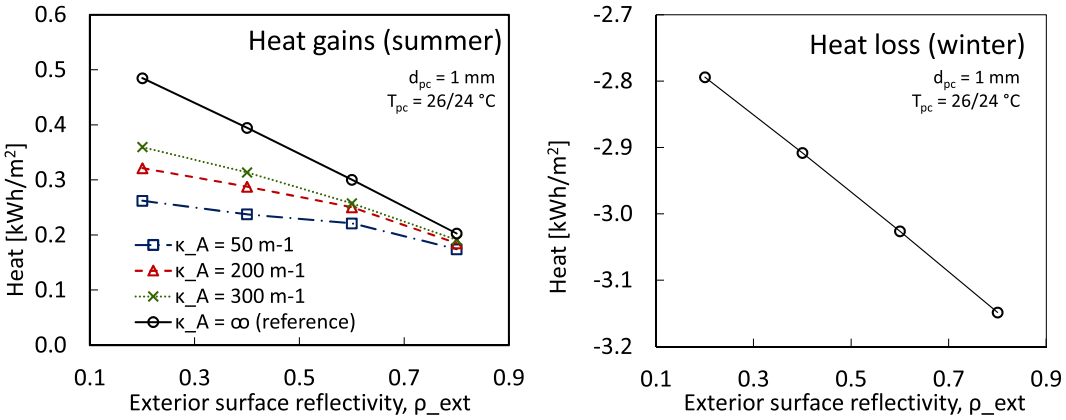

Fig. 8. Thin SS-PCM Layer + Reflector: Total absolute heat gains and losses for the on average warmest and coldest week (i.e. 168 h time period) of the year respectively (undesirable heat exchange). Low κ_A values produce a building enclosure which is less sensitive to the exterior surface reflection during summer conditions. This will allow for the selection of an exterior surface that does not reflect much solar radiation, minimizing heat losses in winter and maximizing heat gains during summer.

The model captures the intended mechanism of the proposed system. Results indicate that the temperature of the back reflector decreases relative to the reference system (which does not exhibit a shift in transparency). Most solar radiation is reflected when the back-reflector becomes exposed, which causes its surface temperature to decrease from 43.7° to 32.0 °C. The system thus operates as intended and has potential to reduce summer heat gains for the proposed building enclosure system. The performance of the system is significantly influenced by the exterior surface reflection coefficient, as can be seen in Fig. 7. When the exterior surface reflection coefficient decreases, less solar irradiance is reflected at the exterior surface and more solar radiation is reflected by the exposed back-reflector. When the exterior surface reflection coefficient increases a significant portion of solar radiation is reflected at the external surface, making the back reflector less influential. Therefore, a low value for ρ_{ext} will be required if the system is intended to deliver benefits of saving energy in both summer and winter conditions. Low exterior surface reflections allow the enclosure to absorb more solar irradiance in winter, yet still allows for reflection of most of the solar irradiance due to an exposed back reflector during warm summer conditions.

Fig. 8a and b, depict the total heat gains and losses for the on average warmest (summer) and coldest (winter) weeks of the year respectively. Results are presented as a function of the exterior reflection coefficient for three different κ_A values. Fig. 8 also depicts the performance of the reference wall, which does not contain the SS-PCM based system and remains opaque. During winter the system remains opaque and only the reference curve exists, there is thus no sensitivity to κ_A. During summer, as κ_A decreases, the influence of ρ_{ext} on summer heat gains decreases, allowing for the selection of a low exterior surface reflection. The latter minimizes heat losses during winter, whilst the exposure of the back reflector minimizes heat gains during summer.

For $\rho_{ext} = 0.2$, the additions of the thin SS-PCM layer based system with a κ_A value of 300 m^{-1} decreases the summer heat gains from 0.48 to 0.36 $\frac{kWh}{m^2}$ (25% reduction), compared to the reference system. This decreases further to 0.26 $\frac{kWh}{m^2}$ (46% reduction) when κ_A drops to 50 m^{-1}. In the case of a higher exterior surface reflectance ($\rho_{ext} = 0.4$), these reductions become 25% and 38% respectively. When both winter and summer conditions are factored in, it becomes clear that a low ρ_{ext} and κ_A are able to create the lowest overall level of undesirable heat exchange. In theory, the proposed system would reach an optimality, with both ρ_{ext} and κ_A approaching zero.

During this evaluation, the thickness of the SS-PCM thin layer is fixed at 1mm. A higher thickness may not be desirable as it will likely increase the amount of solar energy stored as latent heat during warm conditions when the SS-PCM is transparent. The exact thickness could be further optimized based on κ_A and κ_C of the SS-PCM thin-layer. A low κ_C could require a slightly thicker layer due to the necessity to adequately obscure the back reflector in cold conditions. A high κ_A, on the other hand, could require a slightly thinner SS-PCM layer to reduce the level of solar irradiance absorbed within the layer during warm conditions.

4.2. SS-PCM foam system

Fig. 9 shows the influence of foam void-ratio and attenuation coefficient on the undesirable heat gains and losses, with the total heat gains and losses plotted as a function of the foam void-ratio for a summer and winter design week. Results indicate that winter heat losses decrease relative to the reference case (i.e. becoming less negative) when the SS-PCM foam void-ratio increases. The system with lower attenuation coefficient also outperforms the system with higher attenuation coefficient for the winter regardless of foam density. This trend holds true for a case when the SS-PCM phase transition temperature is around 24/26 °C. A lower attenuation coefficient allows solar irradiance to be absorbed deeper into the SS-PCM foam. On the other hand, the system with high attenuation coefficient absorbs heat earlier and is able to store all available thermal energy regardless of foam void ratio.

To assess the influence of the SS-PCM transition temperature we have also modeled a system with a lower phase transition temperature (around −1/1 °C) and low (crystalline) attenuation coefficient (500 1/m). Results indicate that such a system outperforms the reference case (winter) and other SS-PCMs with higher transition temperature for foam void ratios less than 0.75. However, when the foam void ratio increases beyond 0.75 the performance of this system starts to decline. Beyond a foam void ratio of about 0.85 this system performs worse than the reference or other SS-PCM cases. During winter and at lower attenuation coefficient, solar energy penetrates deeper into the SS-PCM foam and heat becomes entrapped as more insulating SS-PCM foam slows the conductive heat losses outwards. When the phase transition temperature of the SS-PCM decreases from 24/26 °C to −1/1 °C, more heat is stored as latent heat since the temperature of the SS-PCMs rises above its phase transition temperature during daytime. A lower melting temperature allows the system to store solar energy as latent heat during the day when system temperatures reaches above freezing. The system with higher transition temperature, on the other hand, only stores sensible heat during winter as its temperature never exceeds phase transition temperature. The ability to store latent heat during a cold winter day thus allows the sys-

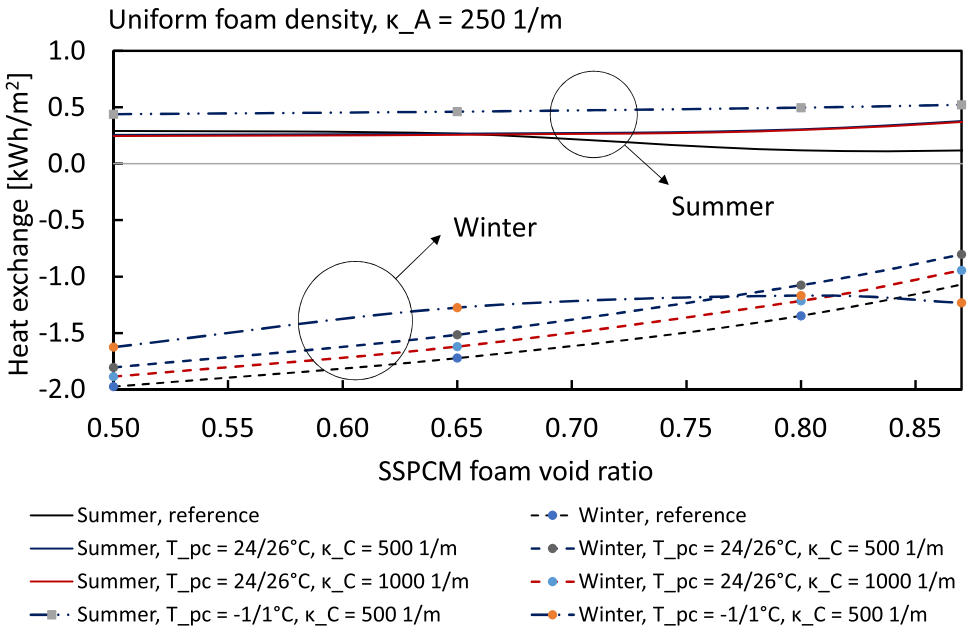

Fig. 9. Heat loss and gains during the on average coldest and warmest week (i.e. 168 h time period) respectively as a function of the SS-PCM foam's void ratio. Slight levels of translucency of the SS-PCM foam increase winter heat gains. An absorption coefficient, κ_C, of 500m^{-1} significantly reduces winter energy losses. During summer conditions, on the other hand, heat gains are above the reference level and are therefore increased because of the system. Although the latent heat keeps this jump to a minimum, which requires a high density foam, or a low foam void ratio.

tem to offset losses at night, which increases performance. This explains why a system with lower melting temperature and/or attenuation coefficient performs better. These effects diminish however beyond a foam void ratio 0.75 since less latent thermal storage capacity is available. In this case, the thermal conductivity of the system starts to dominate the heat transfer process and outweighs the latent heat storage capacity.

Summer performance: During summer conditions, the system with cellular SS-PCM performs marginally better compared to the reference case for a void ratio below 0.65. However, undesirable heat gains in summer increase significantly at foam void ratios above 0.65. This is due to the lower availability of latent heat capacity as the amount of SS-PCM diminishes with increasing void ratio. More latent heat capacity allows for a reduction in temperature peaks within the building enclosure.

Results in Fig. 9 show that the attenuation coefficient has little influence on the systems performance during summer (the case with a transition temperature around 24/26 °C). However, in order to prevent an overheating scenario it is also important to limit the attenuation exhibited by the foam, essentially allowing for more absorption near exterior surface when the SS-PCM is amorphous. The influence of attenuation on heat gains during the summer are presented in Fig. 10. An amorphous attenuation as high as possible, e.g. $\kappa_A = 350\text{m}^{-1}$ or higher, seems to prevent significant overheating, especially when significant latent heat is available. A higher foam void ratio requires a slightly higher attenuation to prevent excess heat gains, as less latent heat capacity can be depended on. To assess the influence of the SS-PCM transition temperature in summer we have also modeled a system with a lower phase transition temperature (around $-1/1\,^{\circ}\text{C}$) and low (crystalline) attenuation coefficient (500 1/m). Such a system performs much worse in summer compared to the reference case and other SS-PCMs. In this design case the SS-PCM is always above phase transition temperature (transparent), which leads to excessive heat gain as solar energy becomes entrapped in the SS-PCM foam. The addition of surface features to control excessive solar heat gain may alleviate some of these problems in summer, while retaining the benefits of a lower phase transition temperature in winter.

From Figs. 9 and 10 it becomes clear that a high foam void ratio is desirable in winter as it enhances the entrapment of heat energy. A lower foam void ratio is desirable in summer conditions as it increases thermal conductivity and latent heat capacity, thus stimulating night cooling. As a compromise, it might be prudent to implement a non-uniform foam void ratio as shown in Fig. 6. A higher foam void ratio at the exterior surface of the enclosure will allow for the absorption of solar irradiance and will prevent heat losses due to a lower thermal conductivity. A lower foam void ratio close to the absorber wall offers better latent heat storage capacity, thus preventing high temperature peaks. The effect of a linear foam void ratio distribution, on temperatures observed at the absorber, is plotted in Fig. 11, and is compared to the results of other void ratio scenarios. A constant high foam void ratio leads to significant temperature peaks, of up to 32 °C observed during summer conditions, whilst varying the foam void ratio linearly from 0.95 to 0.65 decreases the temperature significantly, bringing it close to the curve that represents a constant void foam ratio of 0.65.

A system with linear distribution of the foam void ratio, as described above, performs slightly worse in winter conditions when compared to a system with a constant high void ratio (low density foam). In Fig. 12 a comparison is made with both high and low foam void ratio cases. The case of the linear distribution of the foam void ratio sits roughly in between the cases with low and high foam void ratios. We assumed that a high void ratio δ leads to a slightly higher attenuation coefficient in the amorphous state due to the dominance of absorption in this phase, and a slightly lower attenuation coefficient in the crystalline state, due the dominance of scattering in this phase.

During our evaluation the thickness of the SS-PCM foam based facade system was fixed at 50 mm; and the system was used in combination with a 75 mm conventional thermal insulation backing layer. Results will be different when other system thicknesses are evaluated, or when the technology is used in combination with other wall construction types. Other climates and orientations will

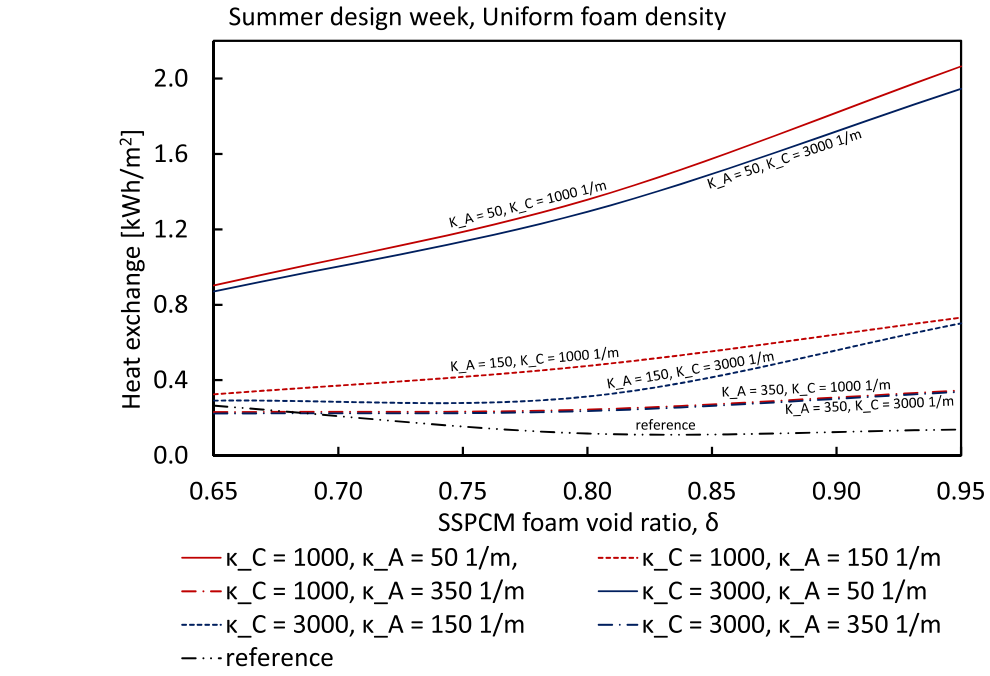

Fig. 10. Heat gains during the on average warmest week as a function of the SS-PCM foam's void ratio for different levels of translucency. When the SS-PCM foam transitions to an amorphous state, the translucency of the foam becomes critical. A low absorption coefficient (high translucency) would increase summer heat gains, whilst higher absorption coefficients deliver heat gains that can still be buffered well by the latent heat capacity.

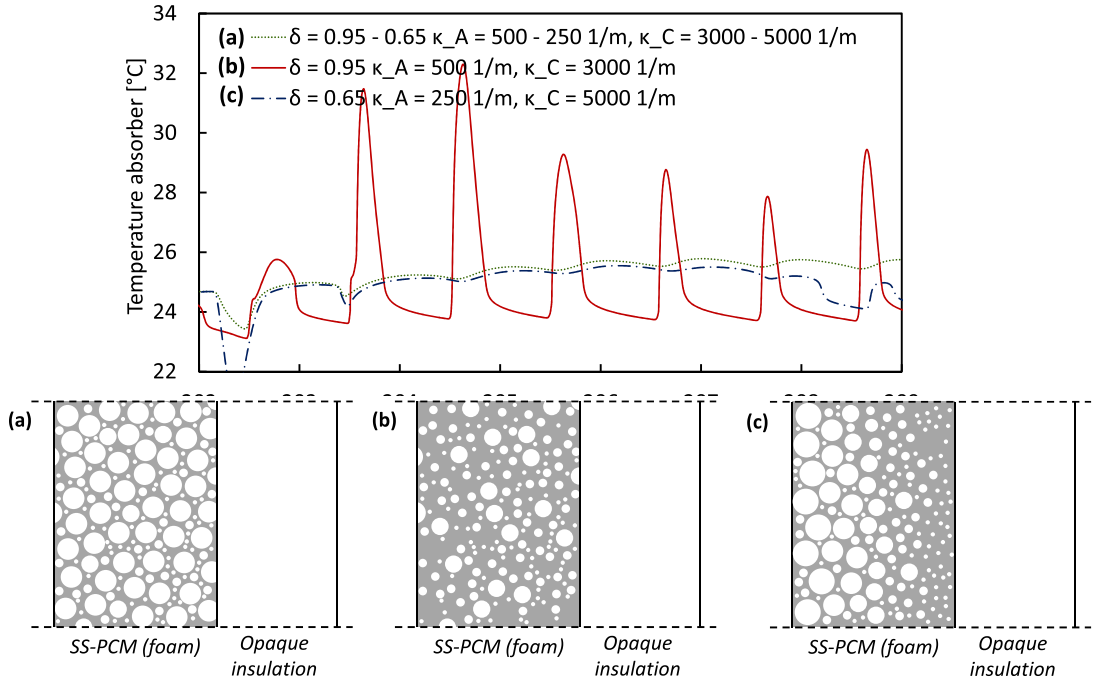

Fig. 11. Absorber temperature during the on average warmest week of the year. (a) A high SS-PCM foam void ratio delivers high diurnal temperature peaks, in other words, not enough latent heat capacity remains available at these low densities. (b) A low SS-PCM foam void ratio delivers low diurnal temperature peaks, (c) A linear distribution of the foam void ratio, ranging from high to low foam void ratio's starting at the exterior surface, greatly reduces temperature peaks, yet is still able to decrease winter heat losses. The latter can be seen in Fig. 12.

likely lead to different optimal solutions. Despite the multitude of performance influencing variables, our results indicate that optimal solutions can be identified that perform better compared to the reference case. A high void ratio seems preferred in heating dominated situations, while a low void ratio seems preferred in cooling dominated situations. Our results indicate that a gradient in the foam void ratio provides better performance overall year round in a central Massachusetts mixed climate type. Attenuation also plays an important role in the seasonal performance, with lower attenuation outperforming systems with higher attenuation in heating dominated situations.

5. Discussion

The thin SS-PCM layer system performs as intended in the FEM simulations. Simulation results indicate that summer heat gain can

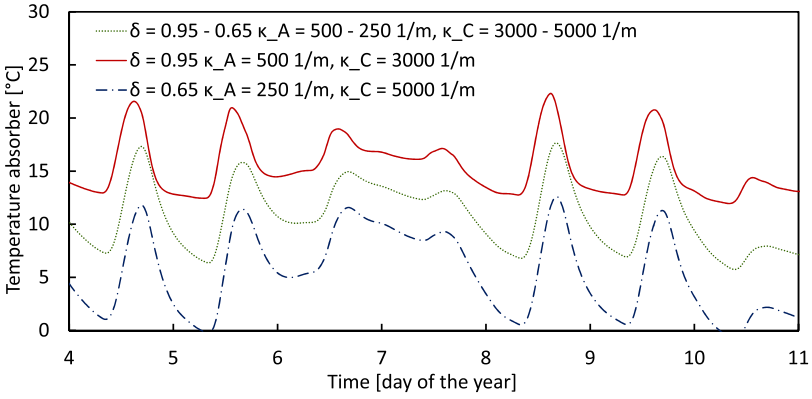

Fig. 12. Absorber temperature during the on average coldest week of the year. A higher foam void ratio (low density foam) increases the temperature due to better retention of internal solar heat gains. A linear distribution of the foam void ratio, ranging from high to low void ratio's starting at the exterior surface, delivers a temperature curve that sits in between the curve for constant high and low void ratio.

be reduced by 25–38%. A trade-off would probably have to be made between a low exterior surface reflection and a low absorption coefficient. For example, if ρ_{ext} is fixed at 0.4, an increase in κ_A from 50 to 200 m^{-1} would still result in a lower overall heat exchange compared to the baseline which is a permanently opaque wall with the same exterior surface reflection value. If, on the other hand, a κ_A value of 300 m^{-1} has to be maintained, an exterior surface reflection of 0.6 or lower would still result in a decrease in overall undesirable heat exchange. A higher κ_A could be compensated by decreasing the thickness of the SS-PCM thin-layer with variable transparency. Switching the level of transparency in between the phases can result in a system with much better performance in terms of reducing undesirable heat exchange. A transparent-when-cold SS-PCM film combined with a back reflector would allow for maximum absorption of solar irradiance.

An alternative to the previous concept would be to switch from a reflector to an absorber, and have the thin layer of SS-PCM become transparent during cold external conditions, rather than during warm conditions with excess amounts of solar irradiation. This set-up has the potential of being less sensitive to external surface reflections, although this approach will require more material development. If the thin layer of SS-PCM would become opaque with rising temperatures, a low exterior reflection coefficient, due to a white material color, would actually become more beneficial.

The second system, based on SS-PCM foam, also has potential to reduce energy use in buildings, if the right combination of material properties is selected. The SS-PCM foam will likely require a high foam void ratio ($\delta \approx 0.95$, low density foam) at the exterior surface and a low foam void ratio ($\delta \approx 0.65$, high density foam) near the core of the building enclosure. The low density foam allows for a significant reduction of heat gains caused by the internal absorption of solar radiation within the foam, whilst the high density foam in the core exhibits significant latent heat and could prevent overheating. It will also be required to further tune the attenuation of the SS-PCM foam in both phases in order for the system to work favorably in both winter and summer conditions.

6. Conclusions

Two climate responsive building enclosure systems are presented that employ the transparency change and latent heat storage capacity of SS-PCMs as mechanisms to passively control building temperature. Finite Element models were developed to study the performance of these systems under winter and summer conditions for a typical central Massachusetts four season climate, assuming a south facing orientation. Our initial results show that both systems can have a positive impact on building performance.

For the system with a thin layer of SS-PCM and back reflector, results indicate that summer heat gain can be reduced by 38% relative to the reference case. It was shown that a low exterior surface coefficient of the SS-PCM layer with variable transparency improves winter performance, due to higher absorption of solar irradiance. The thin layer of SS-PCM should be as thin as possible, although it should still hide the back reflector during cold periods. A trade-off between the exterior surface reflection and the specific absorption rate (during the semi-transparent state) will likely have to be made. For the system consisting of SS-PCM foam, it was shown that energy savings can be obtained if the right combination of material properties is chosen. A high foam void ratio at the exterior surface and low void ratio near the interior surface seem desirable. Further fine-tuning of the attenuation coefficient and transition temperatures of the SS-PCM will be required to make the system work in both summer and winter conditions. It may also prove beneficial to evaluate the benefits of layered systems that stack SS-PCM's with different attenuation coefficients and phase transition temperatures. More research is needed to evaluate the proposed approaches for different wall orientations and climate types.

As an initial study, the simulations presented here aim to analyze the energy performance of the system during the on average warmest and coldest weeks of the year. In order to gain a more comprehensive overview of potential energy savings and system performance trends, future simulations should explore system performance over an annual time period, for different climate types, and for multiple building enclosure orientations. These studies will provide more insight into the nuanced performance profiles of these systems during the so-called "shoulder months".

Future studies should include whole-building energy modeling efforts to elucidate potential energy savings at building level.

Acknowledgments

Support from the National Science Foundation, award number CMMI-1662903 & 1662675, Directorate for Engineering, Division of Civil, Mechanical and Manufacturing Innovation (CMMI), Structural and Architectural Engineering and Materials program (SAEM), is much appreciated.

References

[1] J. Berry, J. Michaels, Annual Energy Review 2011, U.S. Energy Information Administration, Office of Energy Statistics, 2012.

[2] J.D. Kelso, Buildings Energy Data Book, U.S. Department of Energy, Buildings Technologies Program, Energy Efficiency and Renewable Energy, 2011.
[3] S.B. Sadineni, S. Madala, R.F. Boehm, Passive building energy savings: a review of building envelope components, Renew. Sustain. Energy Rev. 15 (2011) 3617–3631.
[4] E. Rodriguez-Ubinas, C. Montero, M. Porteros, S. Vega, I. Navarro, M. Castillo-Cagigal, et al., Passive design strategies and performance of net energy plus houses, Energy Build 83 (2014) 10–22.
[5] R.C.G.M. Loonen, M. Trka, D. Cstola, J.L.M. Hensen, Climate adaptive building shells: state-of-the-art and future challenges, Renew. Sustain. Energy Rev. 25 (2013) 483–493.
[6] M.F. Hordeski, Dictionary of Energy Efficiency Technologies, Fairmont Press Inc., Lilburn, GA, 2004.
[7] O. Saadatian, K. Sopian, C.H. Lim, N. Asim, M.Y. Sulaiman, Trombe walls: a review of opportunities and challenges in research and development, Renew. Sustain. Energy Rev. 16 (2012) 6340–6351.
[8] N.D. Kaushika, K. Sumathy, Solar transparent insulation materials: a review, Renew. Sustain. Energy Rev. 7 (2003) 317–351.
[9] M.S. Sharma, N.D. Kaushika, Design and performance characteristics of honeycomb solar pond, Energy Convers. Manag. 27 (1987) 111–116.
[10] G.M. Wallner, R. Hausner, H. Hegedys, H. Schobermayr, R.W. Lang, Application demonstration and performance of a cellulose triacetate polymer film based transparent insulation wall heating system, Sol. Energy 80 (2006) 1410–1416.
[11] J. Cadafalch, R. Cónsul, Detailed modelling of flat plate solar thermal collectors with honeycomb-like transparent insulation, Sol. Energy 107 (2014) 202–209.
[12] M.A. Shameri, M.A. Alghoul, K. Sopian, M. Zain, M. Fauzi, O. Elayeb, Perspectives of double skin faade systems in buildings and energy saving, Renew. Sustain. Energy Rev. 15 (2011) 1468–1475.
[13] E. Gratia, A. De Herde, Natural cooling strategies efficiency in an office building with a double-skin faade, Energy Build 36 (2004) 1139–1152.
[14] H.Y. Chan, S.B. Riffat, J. Zhu, Review of passive solar heating and cooling technologies, Renew. Sustain. Energy Rev. 14 (2010) 781–789.
[15] J. Shen, S. Lassue, L. Zalewski, D. Huang, Numerical study on thermal behavior of classical or composite trombe solar walls, Energy Build 39 (2007) 962–974.
[16] B. Zamora, A.S. Kaiser, Thermal and dynamic optimization of the convective flow in trombe wall shaped channels by numerical investigation, Heat Mass Transf. 45 (2009) 1393–1407.
[17] H. Onbasioglu, A.N. Egrican, Experimental approach to the thermal response of passive systems, Energy Convers. Manag. 43 (2002) 2053–2065.
[18] C.M. Lai, S. Hokoi, Solar faades: a review., Build Environ. 91 (2015) 152–165.
[19] G. Quesada, D. Rousse, Y. Dutil, M. Badache, S. Hall, A comprehensive review of solar facades. opaque solar facades, Renew. Sustain. Energy Rev. 16 (2012) 2820–2832.
[20] M.S. Buker, S.B. Riffat, Building integrated solar thermal collectors a review, Renew. Sustain. Energy Rev. 51 (2015) 327–346.
[21] G. Quesada, D. Rousse, Y. Dutil, M. Badache, S. Hall, A comprehensive review of solar facades. transparent and translucent solar facades, Renew. Sustain. Energy Rev. 16 (2012) 2643–2651.
[22] L.D.G. Samuel, S.S.M. Nagendra, M.P. Maiya, Passive alternatives to mechanical air conditioning of building: a review, Build Environ 66 (2013) 54–64.
[23] R.V. Ralegaonkar, R. Gupta, Review of intelligent building construction: a passive solar architecture approach, Renew. Sustain. Energy Rev. 14 (2010) 2238–2242.
[24] S. Stevanovi, Optimization of passive solar design strategies: a review, Renew. Sustain. Energy Rev. 25 (2013) 177–196.
[25] J. Heier, C. Bales, V. Martin, Combining thermal energy storage with buildings a review, Renew. Sustain. Energy Rev. 42 (2015) 1305–1325.
[26] R. Baetens, B.P. Jelle, A. Gustavsen, Phase change materials for building applications: a state-of-the-art review, Energy Build 42 (2010) 1361–1368.
[27] N. Soares, J.J. Costa, A.R. Gaspar, P. Santos, Review of passive PCM latent heat thermal energy storage systems towards buildings energy efficiency, Energy Build 59 (2013) 82–103.
[28] L.F. Cabeza, A. Castell, C. Barreneche, A. de Gracia, A.I. Fernndez, Materials used as PCM in thermal energy storage in buildings: a review, Renew. Sustain. Energy Rev. 15 (2011) 1675–1695.
[29] L.A. Chidambaram, A.S. Ramana, G. Kamaraj, R. Velraj, Review of solar cooling methods and thermal storage options, Renew. Sustain. Energy Rev. 15 (2011) 3220–3228.
[30] A.M. Khudhair, M.M. Farid, A review on energy conservation in building applications with thermal storage by latent heat using phase change materials, Energy Convers. Manag. 45 (2004) 263–275.
[31] A. Fallahi, G. Guldentops, M. Tao, S. Granados-Focil, S.V. Dessel, Review on solid-solid phase change materials for thermal energy storage: molecular structure and thermal properties, Appl. Therm. Eng. 127 (2017) 1427–1441.
[32] D.K. Benson, J.D. Webb, R.W. Burrows, J.D.O. McFadden, C. Christensen, Materials Research for Passive Solar Systems: Solid-state Phase-change Materials, U.S. Department of Energy - Solar Energy Research Institute, 1985.
[33] K. Pielichowska, K. Pielichowski, Biodegradable PEO/cellulose-based solid-solid phase change materials, Polym. Adv. Technol. 22 (2011) 1633–1641.
[34] C.A. Whitman, M.B. Johnson, M.A. White, Characterization of thermal performance of a solid-solid phase change material, di-n-hexylammonium bromide, for potential integration in building materials, Thermochim Acta 531 (2011) 54–59.
[35] T.M. Wójcik, M. Wojda, T.M. Wójcik, R. Pastuszko, Novel solid solid phase change material based on polyethylene glycol and cellulose used for temperature stabilisation, MATEC Web Conf. 18 (2014) 1–4.
[36] L. Bianco, Y. Cascone, F. Goia, M. Perino, V. Serra, Responsive glazing systems: characterisation methods, summer performance and implications on thermal comfort, Sol. Energy 158 (2017) 819–836.
[37] L. Bianco, Y. Cascone, F. Goia, M. Perino, V. Serra, Responsive glazing systems: characterisation methods and winter performance, Sol. Energy 155 (2017) 372–387.
[38] X. Ye, Y. Luo, X. Gao, S. Zhu, Design and evaluation of a thermochromic roof system for energy saving based on poly(n-isopropylacrylamide) aqueous solution, Energy Build 48 (2012) 175–179.
[39] C.G. Granqvist, Fenestration for reducing building cooling needs: an introduction to spectral selectivity, thermochromics, and electrochromics, in: Eco-efficient Materials for Mitigating Building Cooling Needs, 2015, pp. 441–471.
[40] J.R. Howell, M.P. Mengüç, R. Siegel, Thermal Radiation Heat Transfer, sixth ed., Taylor and Francis Group, LLC., Florida, 2016.
[41] T.L. Bergman, A.S. Lavine, F.P. Incropera, D.P. Dewitt, Fundamentals of Heat and Mass Transfer, seventh ed., Wiley and Sons, Inc., New York, 2011.
[42] H.R.N. Jones, Radiation Heat Transfer, Oxford University Press, Oxford, 2000.
[43] G.B. Cordon, M.G. Lagorio, Absorption and scattering coefficients: a biophysical-chemistry experiment using reflectance spectroscopy, J. Chem. Educ. 84 (2007) 1167–1170.
[44] N. Yamada, S. Fujimura, Nondestructive measurement of chlorophyll pigment content in plant leaves from three-color reflectance and transmittance, Appl. Opt. 30 (1991) 3964–3973.
[45] A.E. Vargas, G.A. Niklasson, Applicability conditions of the kubelka-munk theory, Appl. Opt. 36 (1997) 5580–5586.
[46] W.A. Allen, A.J. Richardson, Interaction of light with a plant canopy, Appl. Opt. 58 (1968) 1023–1028.
[47] L. Fukshansky, N. Fukshansky-Kazarinova, A.M.v. Remisowsky, Estimation of optical parameters in a living tissue by solving the inverse problem of the multiflux radiative transfer, Appl. Opt. 30 (1991) 3145–3153.
[48] N.B. Hutcheon, G.O.P. Handegord, Building Science for a Cold Climate, National Research Council of Canada, Montreal, 1995.
[49] J. Meeus, Astronomical Algorithms, Willmann-Bell Inc., Richmond, Virginia, 1991.
[50] R.S. Perez, R. Seals, P. Ineichen, R. Stewart, D. Menicucci, A new simplified version of the Perez diffuse irradiance model for tilted surfaces, Sol. Energy 39 (1987) 221–231.
[51] R. Perez, R. Stewart, R. Seals, T. Guertin, The Development and Verification of the Perez Diffuse Radiation Model, Atmospheric Sciences Research Center, 1988.
[52] G.N. Walton, Thermal Analysis Research Program Reference Manual, National Bureau of Standards, 1983.
[53] G. Clark, C. Allen, The Estimation of Atmospheric Radiation for Clear and Cloudy Skies, in: Proceedings of the 2nd National Passive Solar Conference (AS/ISES), pp. 675–678.
[54] M.G. Lawrence, The relationship between relative humidity and the dewpoint temperature in moist air: a simple conversion and applications, Bull. Am. Meteorol. Soc. 86 (2005) 225–233.
[55] M. Emel, M. Abadie, N. Mendes, New external convective heat transfer coefficient correlations for isolated low-rise buildings, Energy Build 39 (2007) 335–342.
[56] R.D. Judkoff, J.S. Neymark, Building Energy Simulation Test (BESTEST) and Diagnostic Method, National Renewable Energy Laboratory, Colorado, 1995.
[57] T.C. Min, L.F. Schutrum, G.V. Parmelee, J.D. Vouris, Natural convection and radiation in a panel heated room, in: Heating Piping and Air Conditioning, May 1956, pp. 153–160.
[58] L.R. Glicksman, Heat transfer in foams, Low Density Cellular Plastics, Chapman & Hall, London, 1994.